

Panoster: End-to-end Panoptic Segmentation of LiDAR Point Clouds

Stefano Gasperini^{1,2} Mohammad-Ali Nikouei Mahani² Alvaro Marcos-Ramiro²
Nassir Navab^{1,3} Federico Tombari^{1,4}

Abstract—Panoptic segmentation has recently unified semantic and instance segmentation, previously addressed separately, thus taking a step further towards creating more comprehensive and efficient perception systems. In this paper, we present Panoster, a novel proposal-free panoptic segmentation method for point clouds. Unlike previous approaches relying on several steps to group pixels or points into objects, Panoster proposes a simplified framework incorporating a learning-based clustering solution to identify instances. At inference time, this acts as a class-agnostic semantic segmentation, allowing Panoster to be fast, while outperforming prior methods in terms of accuracy. Additionally, we showcase how our approach can be flexibly and effectively applied on diverse existing semantic architectures to deliver panoptic predictions.

I. INTRODUCTION

Scene understanding is a fundamental task for autonomous vehicles. Panoptic segmentation (PS) [1] combines semantic and instance segmentation, enabling a single system to develop a more complete interpretation of its surroundings. PS is based on the distinction between *stuff* and *thing* classes [1], with the former being uncountable and amorphous regions, such as *road* and *vegetation*, and the latter standing for countable objects, such as *people* and *cars*. The two have been addressed separately for decades, leading to significantly different approaches: *stuff* classifiers are typically based on fully convolutional networks [2], while *thing* detectors often rely on region proposals and the regression of bounding-boxes [3]. Tackling semantic and instance segmentation jointly with PS allows to save costly and limited resources [4].

Since the introduction of PS, several approaches have been proposed to address this new task. While most focused on images [4–6] or RGBD data [7, 8], only a handful of methods used LiDAR point clouds [9, 10]. LiDAR sensors have proven to be particularly useful for self-driving cars, capturing precise distance measurements of the surrounding environment. Segmenting LiDAR point clouds is a crucial step for interpreting the scene. Compared to image pixels, LiDAR point clouds pose various challenges: they are unstructured, unordered, sparse, and irregularly sampled.

In this paper, we introduce a novel proposal-free approach for panoptic segmentation of LiDAR point clouds. We name

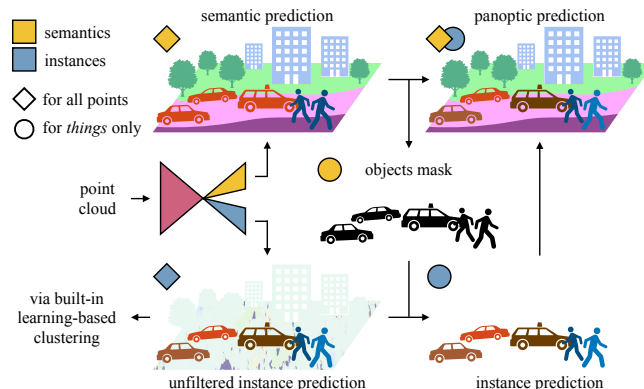


Fig. 1. Proposed Panoster framework. A semantic class and an instance ID are predicted for every point, then filtered and combined for panoptic segmentation.

our method Panoster, standing for panoptic clustering. Panoster brings panoptic capabilities to semantic segmentation networks by adding an instance branch trained to resolve objects with a learning-based clustering method [11]. Unlike existing proposal-free approaches [6, 10], Panoster, thanks to its clustering solution integrated in the model, does not need further groupings to form objects, as it outputs instance IDs straight away from the network.

The contributions of this paper can be summarized as follows:

- We introduce a new proposal-free approach for panoptic segmentation, fully end-to-end, flexible and fast, with a small overhead on top of an equivalent semantic segmentation architecture.
- To the best of our knowledge, for the first time in panoptic segmentation, we exploit an entirely learning-based end-to-end clustering approach to separate the instances.
- Our novel instance segmentation acts as class-agnostic semantic segmentation, is free from any thresholds, and delivers instance IDs directly without requiring further grouping steps.

We apply Panoster on the challenging task of panoptic segmentation for LiDAR 3D point clouds, outperforming in a fraction of the time state-of-the-art methods. Furthermore, we show the flexibility of Panoster by deploying it on both projection-based and point-based architectures, making it the first panoptic method to consume LiDAR 3D points directly.

¹ Computer Aided Medical Procedures, Technical University of Munich, Munich, Germany. stefano.gasperini@tum.de

² BMW Group, Munich, Germany.

³ Computer Aided Medical Procedures, Johns Hopkins University, Baltimore, USA.

⁴ Google, Zurich, Switzerland.

II. RELATED WORK

In this section, we provide a brief overview of existing approaches, and highlight overlaps and differences with Panoster.

A. Semantic Segmentation

Depending on the input representation, semantic segmentation methods can be grouped into projection-based and point-based. Projection-based approaches eliminate the challenging irregularities of 3D points by projecting them into an intermediate grid. This grid representation can be made of voxels [12, 13] or pixels [14, 15], allowing the use of 3D or 2D convolutions. While the former projection tends to be highly inefficient for this task, the latter can count on state-of-the-art methods from image segmentation, albeit discarding valuable geometric information by transitioning from 3D to 2D.

PointNet [16] pioneered point-based methods and deep learning on point clouds. They used multilayer perceptrons (MLP) to learn features from each point, then aggregated with a global max-pooling. This idea was further developed in [17–19]. More recent approaches, such as KPConv [20] and SpiderCNN [21] have focused on creating new convolution operations for points. KPConv [20] extended the idea of 2D image kernels to 3D points, by defining an operation which derives new 3D points from the multiplication of input 3D point features with flexible kernel weights. Recently, hybrid approaches have been developed [22, 23], combining point and projection-based solutions.

Our method Panoster extends semantic segmentation approaches to panoptic segmentation. In this paper we apply Panoster on KPConv [20] and SalsaNext [15], representative of point-based and projection-based categories respectively.

B. Instance Segmentation

Instance segmentation methods can be divided into detection-based and clustering-based. The former was established in the image domain by Mask R-CNN [24] which has two stages: region proposals are extracted, refined into bounding boxes, and segmented with a pixel-level mask to identify the objects. Clustering-based approaches learn an embedding space in which instances can be easily clustered [25, 26]. These methods were extended to point clouds in [27–29].

Instead, Panoster clusters instances with a learning-based method, without using embeddings. We address instance segmentation as class agnostic semantic segmentation, directly predicting instance IDs for each point.

C. Panoptic Segmentation

PS methods can be divided into two categories: proposal-based and proposal-free. The vast majority are from the image domain, of which the larger stake are proposal-based or top-down methods [4, 5, 30, 31]: two-stage approaches, which are usually based on the well-known Mask R-CNN [24]. They rely on the detection of *things* first, followed by a refinement step and a *stuff* segmentation

branch to fill the remaining regions. Instead, proposal-free or bottom-up methods are single-stage and follow the opposite direction. They segment the scene semantically, and cluster the instances within the predicted *thing* segments. DeeperLab [32] was the first of this kind, regressing objects center and corners from images. SSAP [33] used a cascaded graph partition module to group pixels into instances according to a pixel-pair affinity pyramid. Panoptic-DeepLab [6] simplified this concept by predicting the instance center locations, and using a Hough-Voting scheme to group the pixels to the closest center.

While PS received a lot of attention in the image domain, PS on LiDAR point clouds is yet broadly unexplored, due to the only recent introduction of a suitable public dataset [34]. In [34] strong baselines were proposed by combining state-of-the-art semantic segmentation [14, 20] and object detection [19]. PanopticTrackNet [9] extended [4] to LiDAR point clouds: it is top-down, based on Mask R-CNN [24] to resolve the instances. Additionally, a new tracking head delivers temporally consistent instance IDs. The only existing bottom-up method for LiDAR point clouds is [10], which we denote as LPSAD. It is based on semantic embeddings and, as in [6], the regression of offsets to the object centers, then instances are extracted by an iterative clustering procedure, grouping points according to their center offset prediction. To date, no method managed to outperform the combined baselines proposed in [34].

Panoster is significantly different from existing panoptic approaches. It is the first to use an entirely learning-based clustering technique to resolve the instances. As LPSAD [10], our method is bottom-up and applied on LiDAR point clouds, but compared to it, our instance branch outputs instance IDs directly, without requiring any subsequent grouping steps, rendering it fully end-to-end trainable.

III. PANOSTER

A. Overview

As described in Section II-C, current proposal-free panoptic approaches [6, 10] pair a network with an external grouping technique to form objects. The latter exploits the network predictions, and is required in order to output any meaningful instance IDs. With the proposed Panoster, we simplify by removing this extra step, and incorporating the clustering in the network itself. We achieve this with an entirely learning-based approach, adapted from the signal processing domain [11], to output instance IDs directly, for each point given in input (Section III-C). To obtain panoptic predictions, it is then sufficient to filter out these IDs for all *stuff* points (Section III-D), as shown in Fig. 1. Thanks to custom loss functions, our integrated clustering method instills grouping capabilities right in the model weights. At inference time, these layers process data in the same way as their semantic segmentation counterparts, while pursuing the rather different task of instance segmentation. In Fig. 2 we showcase how our method compares with a typical semantic segmentation network from the architecture perspective, highlighting how each part is trained.

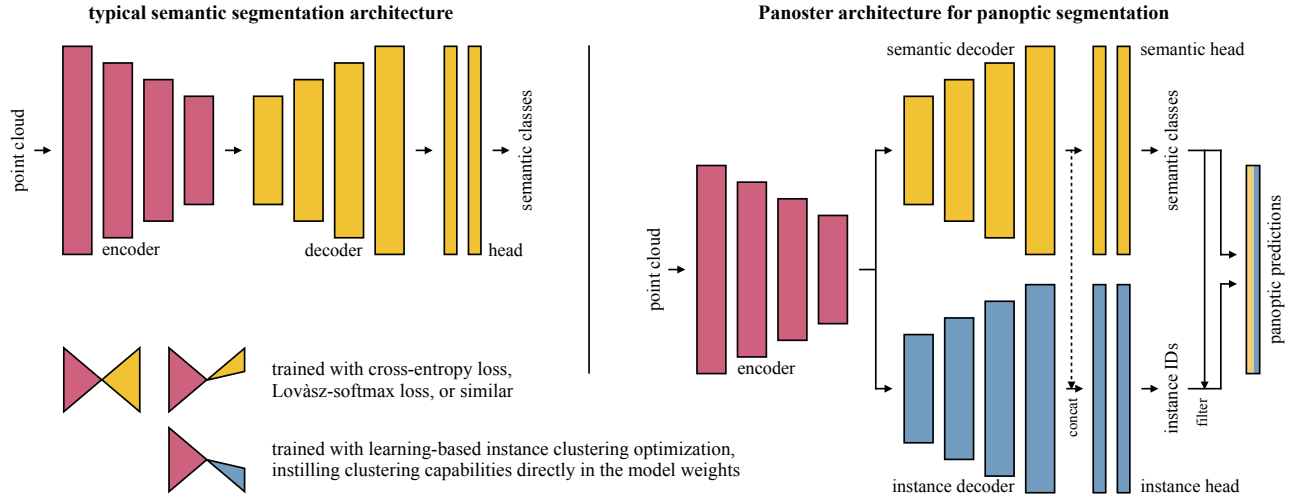


Fig. 2. Conversion of a typical semantic segmentation architecture (left) to Panoster (right). The input is raw 3D points or a 2D spherical projection. During training, gradients do not back-propagate through the dashed line. At inference time, both decoders and heads process data in the same way.

B. Architecture

Panoster consists of the following modules: a shared encoder, decoupled symmetric decoders and heads for the two tasks, mask-based fusion and optional post-processing.

Motivated by [6, 9, 10], we opt for a shared encoder with two separate decoders, each developing its task starting from common features. As can be seen in Fig. 2, the backbone, the semantic decoder and head follow the design of a standard semantic segmentation network, consuming a full 360 degree LiDAR point cloud. In this paper we apply Panoster on KPConv [20] and SalsaNext [15]. We refer to the two variants as PanosterK and PanosterS, respectively. Therefore, depending on the configuration, our framework can be fed with raw 3D points or with a 2D spherical projection.

As shown in Fig. 2, our method has a second decoder and head, dedicated to instance segmentation. The instance decoder uses the same architecture as the semantic one. The difference between the two branches is how they are optimized to tackle the two tasks. Additionally, the input of the instance head is the concatenation of both decoders outputs.

We train the semantic branch to predict both *stuff* and *thing* classes. We use the same objective functions as in [15], namely weighted cross-entropy, and Lovász-softmax loss [35], optimizing the Jaccard index. We weight their sum 0.7 for PanosterK and 1.0 for -S. Moreover, following [6],

| | sample prediction | clusters purity | detected instances | fragmented instances |
|---|-------------------|-----------------|--------------------|----------------------|
| 1 | | 3 ok | 3 ok | 3 ok |
| 2 | | 2 wrong | 1 wrong | 2 wrong |
| 3 | | 1 wrong | 1 wrong | 3 ok |
| 4 | | 12 ok | 3 ok | 3 wrong |

Fig. 3. Sample instance segmentation predictions with analysis on cluster purity, detection and fragmentation.

to improve the accuracy on small or distant *thing* objects, we triple the cross-entropy weight on instances smaller than 100 points for PanosterK. We found this to be not beneficial for -S.

C. Learning-based Instance Clustering

Our instance branch addresses its task as class-agnostic semantic segmentation, making a prediction for each point. In [11] the authors proposed a learning-based clustering method to separate radar signals by source. We adapt this approach to suit the panoptic task: cluster elements are 3D points, and each ground truth cluster represents an object instance. We deploy confusion matrices as control panels for the optimization of pure and non-fragmented clusters. Purity and fragmentation need to be balanced for the best outcome, as described in Fig. 3. By considering the *softmax* probabilities as cluster assignment probabilities, confusion matrices become soft confusion matrices S , allowing for the construction of loss functions. We refer the reader to [11] for further details.

The **impurity loss** L_{imp} in Eq. 1 optimizes clusters purity, shifting from use cases 2 and 3 to 1 and 4 in Fig. 3. We adapt the impurity loss from [11] by considering percentages instead of the amount of points, rendering it robust against the imbalance of cluster sizes:

$$L_{imp} = \frac{\sum Q(S)}{\sum S} \quad (1)$$

$$Q(S) := \{S_i^j / \sum S_i\} : S_i^j \notin M^j(S) \quad \forall i, j$$

where $M(S) := \{\max(S^j) \forall j\}$ is the set of column maxima. Also, with S_i^j we indicate the (i, j) cell of S , sized $G \times N$; with S_i and S^j its i -th row and j -th column; N is the amount of predictable instances; G is the number of ground truth objects.

An additional **fragmentation loss** L_{fr} reduces fragmenta-

TABLE I

PANOPTIC SEGMENTATION COMPARISON ON TEST SET RESULTS OF SEMANTICKITTI. ALL VALUES IN [%] WITH St FOR *stuff* AND Th FOR *thing*.

| Method | PQ | PQ [†] | SQ | RQ | PQ Th | SQ Th | RQ Th | PQ St | SQ St | RQ St | mIoU |
|-------------------------------------|-------------|-----------------|-------------|-------------|------------------|------------------|------------------|------------------|------------------|------------------|-------------|
| RangeNet++ [14] + PointPillars [19] | 37.1 | 45.9 | 75.9 | 47.0 | 20.2 | 75.2 | 25.2 | 49.3 | 76.5 | 62.8 | 52.4 |
| LPSAD [10] | 38.0 | 47.0 | 76.5 | 48.2 | 25.6 | 76.8 | 31.8 | 47.1 | 76.2 | 60.1 | 50.9 |
| KPCConv [20] + PointPillars [19] | 44.5 | 52.5 | 80.0 | 54.4 | 32.7 | 81.5 | 38.7 | 53.1 | 79.0 | 65.9 | 58.8 |
| PanosterK [Ours] | 45.6 | 52.8 | 78.1 | 57.0 | 32.4 | 77.1 | 41.6 | 55.1 | 78.8 | 68.2 | 60.4 |
| PanosterK + <i>post_*</i> [Ours] | 52.7 | 59.9 | 80.7 | 64.1 | 49.4 | 83.3 | 58.5 | 55.1 | 78.8 | 68.2 | 59.9 |

TABLE II

DETAILED CLASS-WISE PQ RESULTS OF SEMANTICKITTI TEST SET. ALL VALUES IN [%].

| Method | PQ | car | truck | bicycle | motorcycle | other vehicle | person | bicyclist | motorcyclist | road | sidewalk | parking | other ground | building | vegetation | trunk | terrain | fence | pole | traffic sign |
|---------------------------|-------------|-------------|-------------|-------------|-------------|---------------|-------------|-------------|--------------|-------------|-------------|-------------|--------------|-------------|-------------|-------------|-------------|-------------|-------------|--------------|
| RangeNet++ + PointP. | 37.1 | 66.9 | 6.7 | 3.1 | 16.2 | 8.8 | 14.6 | 31.8 | 13.5 | 90.6 | 63.2 | 41.3 | 6.7 | 79.2 | 71.2 | 34.6 | 37.4 | 38.2 | 32.8 | 47.4 |
| KPCConv + PointP. | 44.5 | 72.5 | 17.2 | 9.2 | 30.8 | 19.6 | 29.9 | 59.4 | 22.8 | 84.6 | 60.1 | 34.1 | 8.8 | 80.7 | 77.6 | 53.9 | 42.2 | 49.0 | 46.2 | 46.8 |
| PanosterK | 45.6 | 49.6 | 13.7 | 9.2 | 33.8 | 19.5 | 43.0 | 50.2 | 40.2 | 90.2 | 62.5 | 34.5 | 6.1 | 82.0 | 77.7 | 55.7 | 41.2 | 48.0 | 48.9 | 59.8 |
| PanosterK + <i>post_*</i> | 52.7 | 84.0 | 18.5 | 36.4 | 44.7 | 30.1 | 61.1 | 69.2 | 51.1 | 90.2 | 62.5 | 34.5 | 6.1 | 82.0 | 77.7 | 55.7 | 41.2 | 48.0 | 48.9 | 59.8 |

tion, penalizing the S cells responsible for fragments $F(S)$:

$$L_{fr} = \frac{\sum F(S) \odot F(S)}{N}$$

$$F(S) := \{S_i^j\}; S_i^j \in M_i(S) \wedge S_i^j \neq \max(M_i(S)) \quad \forall i, j \quad (2)$$

$$M_i(S) := S_i \cap M(S)$$

In the equation, the numerator is the differentiable equivalent of counting the fragments $F(S)$, thanks to the Hadamard element-wise division \odot . This loss tries to bring use case 4 of Fig. 3 to 1.

The instance branch is trained with a combination of L_{imp} and L_{fr} , weighted 0.2 and 0.05 respectively.

D. Panoptic Segmentation

PS requires a semantic class for each point, as well as instance IDs for *thing* objects. Both branches output a prediction for each point of *stuff* and *thing* classes. As shown in Fig. 1, we extract an object mask from the semantic output. We use this to filter the instance predictions and obtain instance IDs for *things*, assigning *ID 0* to all remaining *stuff* points. We then obtain PS predictions by stacking semantic classes and instance IDs.

Optional post-processing. As described in Section III-C, unlike previous works [6, 10], our instance predictions do not necessarily require further grouping or post-processing. Nevertheless, we explored three different post-processing strategies, as plausibility checks, exploiting 3D information and the synergy between the two tasks. To improve detection and cluster purity, DBSCAN [36] targets the third use case of Fig. 3. We call this strategy *post_splitter*: it splits instances which are too large in space w.r.t. their corresponding predicted semantic classes. Furthermore, to reduce fragmentation, *post_merger* can be deployed to fix the fourth use case of Fig. 3. It uses DBSCAN to cluster the 3D centers of those instances of the same semantic class, which are too close to each other. Finally, with *post_cyclists*, we

turn *bicyclists* who have no *bicycle* nearby, but a *motorbike*, into *motorcyclists*.

IV. EXPERIMENTS

Dataset. We evaluate on the challenging SemanticKITTI [37], which was recently extended [34] by providing instance IDs for all LiDAR scans of KITTI odometry [38]. It contains 23201 full 360 degrees scans for training and 20351 for testing, sampled from 22 sequences from various German cities. We use training sequence 08 as validation split, following the convention. Annotations comprise point-wise labels within 50 meters radius across 22 classes, 19 of which evaluated on the test server: 11 *stuff* and 8 *thing*.

Model training. Experiments are focused mainly on PanosterK, based on KPCConv [20], while showing the flexibility of Panoster by applying it also on SalsaNext [15] with PanosterS. Unless otherwise noted, we used the same training parameters as in [20] for PanosterK and [15] for PanosterS, with the addition of our instance clustering loss functions. To better fit the PS task, we used input point clouds covering the entire scene, instead of small regions as in [20]. At each training iteration, we fed PanosterK with at most 80K points. PanosterK used rigid KPCConv kernels. For PanosterS we used batch size 4 and learning rate 0.001. We implemented our method in PyTorch and trained the models on a single NVIDIA Tesla V100 32GB GPU. We trained PanosterK from scratch for at least 200K iterations. PanosterS was pretrained on semantic segmentation, and fine-tuned on panoptic segmentation for 100K iterations. The PanosterK model submitted to the test server was trained on the entire training set, including the validation set.

Inference. Unlike KPCConv [20], at inference time we fed the whole 50 meters radius scene in a single forward pass, without any test-time augmentation.

TABLE III
 PANOPTIC SEGMENTATION ON THE VALIDATION SET OF
 SEMANTICKITTI. ALL VALUES IN [%].

| Method | PQ | SQ | RQ | PQ Th | RQ Th | mIoU |
|---------------------------|-------------|-------------|-------------|------------------|------------------|-------------|
| RangeNet++ + Pt.P. | 36.5 | 73.0 | 44.9 | 19.6 | 24.9 | 52.8 |
| LPSAD | 36.5 | - | - | - | 28.2 | 50.7 |
| PanopticTrackNet | 40.0 | 73.0 | 48.3 | 29.9 | 33.6 | 53.8 |
| KPConv + Pt.P. | 41.1 | 74.3 | 50.3 | 28.9 | 33.1 | 56.6 |
| PanosterS | 43.5 | 68.6 | 55.2 | 32.6 | 42.3 | 57.8 |
| PanosterS + <i>post_*</i> | 51.1 | 76.9 | 62.1 | 50.5 | 58.6 | 57.8 |
| PanosterK | 48.4 | 73.0 | 60.1 | 39.5 | 50.0 | 60.4 |
| PanosterK + <i>post_*</i> | 55.6 | 79.9 | 66.8 | 56.6 | 65.8 | 61.1 |

Evaluation metrics. We report mean IoU (mIoU) and panoptic quality (PQ) [1] to evaluate semantic and panoptic segmentation, both averaged over all classes. PQ can be seen as the multiplication of segmentation quality (SQ) and recognition quality (RQ) [1], with the former being the mIoU of matched segments and the latter representing the F_1 score, commonly adopted for object detection. Additionally we report the alternative PQ[†] [5], which ignores RQ for *stuff* classes. Since the main focus and contribution of our method within PS is on instance segmentation and clustering, among the various metrics we concentrate on RQTh, which is RQ for *thing* classes.

A. Panoptic Segmentation

We compared Panoster with other PS approaches for LiDAR point clouds, submitting PanosterK to the SemanticKITTI challenge. Two strong baselines were proposed in [34] combining KPConv [20] or RangeNet++ [14] with PointPillars [19], semantic segmentation and object detection methods. Furthermore, we compared with PanopticTrackNet [9] and LPSAD [10], top-down and bottom-up approaches respectively.

Table I shows results on the secret test set. Overall, PanosterK delivered superior performance compared to previous approaches. Despite obtaining worse semantics with a lower SQ, PanosterK’s strengths are its finer clustering and instance segmentation abilities, shown on *thing* classes, resulting in a 2.9 increase in RQTh on top of state-of-the-art KPConv and PointPillars, albeit sharing the same backbone. Considering individual classes, Table II shows that PointPillars [19], which is a strong object detector, performed better than our instance clustering approach on the classes *car*, *truck* and *bicyclist*, while ours prevailed on *person*, *motorcycle* and *motorcyclist*. Nevertheless, compared to the combined approaches, our PanosterK was able to deliver a better panoptic segmentation, while using a single network in a multi-task fashion. LPSAD [10], the only other bottom-up method to date, despite a more complex architecture and a necessary grouping step, achieved significantly lower PQ and RQTh. Overall, we attribute PanosterK performance to the high quality instance segmentation resulting from its built-in learning-based clustering approach. By optimizing the cluster assignments directly for purity and non-fragmentation,

TABLE IV
 ABLATION STUDY ON THE VALIDATION SET OF SEMANTICKITTI, WITH
c FOR *car*, *b* FOR *bicycle* AND *p* FOR *person*. ALL VALUES IN [%].

| Method | PQ | RQ Th | RQ ^c | RQ ^b | RQ ^p | mIoU |
|--------------------------|-------------|------------------|-----------------|-----------------|-----------------|-------------|
| KPConv + instance | 45.9 | 45.2 | 53.3 | 42.4 | 51.2 | 58.3 |
| + extra decoder | 45.2 | 43.5 | 65.4 | 37.5 | 60.8 | 59.0 |
| + % conf. matrix | 47.6 | 49.3 | 75.5 | 47.1 | 67.1 | 60.0 |
| + Lovász-softmax | 48.3 | 49.6 | 74.2 | 38.9 | 70.1 | 61.1 |
| + small inst. 3x | 48.5 | 49.4 | 75.0 | 40.0 | 75.1 | 60.2 |
| + skip= PanosterK | 48.4 | 50.0 | 79.5 | 50.6 | 74.1 | 60.4 |
| + <i>post_splitter</i> | 50.4 | 54.4 | 87.4 | 60.1 | 85.4 | 60.4 |
| + <i>post_merger</i> | 54.7 | 62.9 | 95.3 | 60.9 | 87.6 | 60.4 |
| + <i>post_cyclists</i> | 55.6 | 65.8 | 95.3 | 60.9 | 87.6 | 61.1 |

PanosterK could achieve good instance segmentation, without affecting semantic accuracy. Furthermore, applying our optional post processing techniques *post_** (Section III-D) increased PQ by 7.1 reaching 52.7, with RQTh at 58.5. More details on this are presented in Section IV-B.

We report validation set results in Table III, including PanopticTrackNet [9], which has no test entry to date. We add validation results of the combined approaches [34], as outlined in [9]. Although our projection-based PanosterS, outperformed previous methods, our point-based PanosterK delivered even better results. We attribute this to the direct consumption of 3D points, which leads to a better use of geometric information, fundamental when separating instances in 3D space.

B. Ablation Study

In Table IV, we summarize an ablation study to assess the impact of different components of PanosterK on PS.

Instance improvements. Although using a single decoder achieved higher PQ and RQTh, dedicated decoders led to a significantly better RQ on *car* and *person*, while improving semantic performance on mIoU, motivating our choice for the latter configuration. As described in Section III-C, compared to the instance clustering approach adapted from [11], we increased the robustness against unbalanced cluster sizes. This change, shown in Table IV as “% conf. matrix”, largely improved the predictions, preventing closer and larger objects, in terms of point counts, from dominating smaller and further ones in the clustering process. Furthermore, we added a skip connection from semantic to instance head, which led to a higher RQTh, with better detection for the classes *car* and *bicycle*.

Semantic improvements. Since Panoster is a bottom-up method, to avoid errors propagating through the *things* mask, precise semantic segmentation is key for high quality panoptic outputs. Towards this end, we applied the Lovász-softmax loss and we limited false negatives by increasing the weight of small instances (denoted by “small inst. 3x” in Table IV). The former had a positive impact on mIoU, PQ and RQTh. The latter, despite decreasing mIoU, increased precision on smaller *thing* classes, such as *person*.

Number of predictable clusters N. For all experiments we set N equal to 60, higher than the amount of objects found

across the dataset in a single scan. This number can be seen equivalent to the amount of bounding boxes processed in an object detector [24]. Two architectures using $N = \{60, 90\}$ resulted in a PQ difference of 0.1, showing Panoster insensitivity against N .

Post-processing. As it can be seen in Tables I, II, III and IV, our optional *post_** strategies (Section III-D) bring significant improvements to Panoster predictions. They complement our model, fixing its clustering errors through plausibility checks by exploiting 3D data and the task duality of PS. The largest improvement is brought by *post_merger*, which joins close instances likely to be part of the same object, divided by the model or by *post_splitter*.

C. Runtime Comparison

Our PanosterK model runs on 80K points at 58 FPS at inference time on a NVIDIA GTX 1080 8GB GPU, which is 3 FPS (i.e. 5%) slower than its semantic counterpart. Therefore, Panoster brings panoptic capabilities with a relatively small overhead with respect to semantic segmentation networks. In comparison, LPSAD, the previously fastest existing method for PS on LiDAR point clouds, runs at 11.8 FPS [10]. Panoster’s built-in learning-based clustering avoids cumbersome grouping strategies to form instances, allowing it to be fast. Moreover, Panoster is more efficient than the combined methods, which require three networks, i.e., one for semantic segmentation, and two for detecting smaller and larger objects [34].

D. Qualitative Results

In Fig. 4 we showcase PanosterK predictions on two complex validation scenes, with road intersections and several objects. Each shows the whole 50m radius scan. Despite point sparsity, predictions do not degenerate by increasing the distance from the sensor. Additionally, Panoster is able to distinguish neighboring objects, assigning them different IDs (i.e. colors), as in detail 3 of Fig. 4. Although in challenging scenes, such as the bottom one in the figure, it reuses the same ID for multiple instances, these can be fixed via post-processing as matching IDs are found only in distant objects. We attribute this behavior to the relatively low amount of instances and complex scenes in most training samples.

V. CONCLUSION

In this paper we proposed Panoster: a fast, flexible, and proposal-free panoptic segmentation method, which we evaluated on the challenging LiDAR-based SemanticKITTI dataset, across two different input representations. Panoster outperformed state-of-the-art approaches, while also being simpler and faster. Our method directly delivers instance IDs with a learning-based clustering solution, embedded in the model and optimized for pure and non-fragmented clusters. With its small overhead, Panoster constitutes a valid end efficient approach to extend existing and upcoming semantic methods to perform panoptic segmentation.

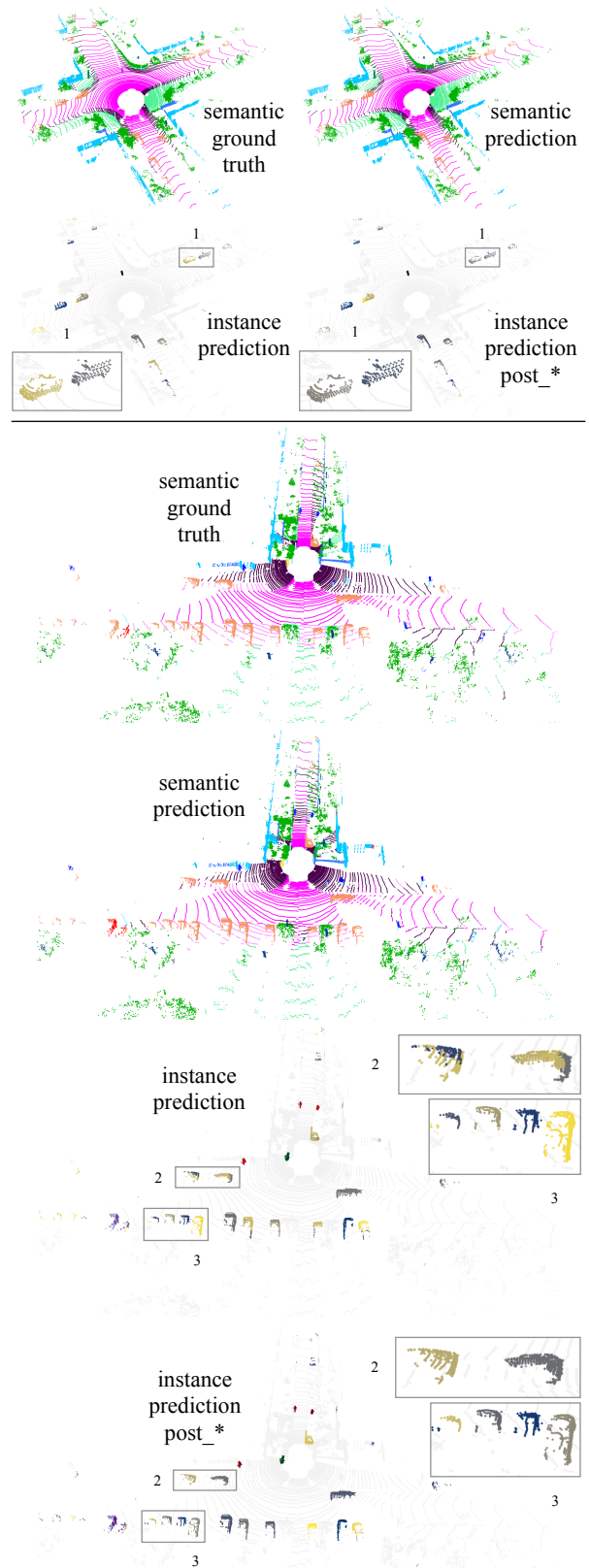


Fig. 4. Qualitative results of PanosterK on two challenging samples from the validation set of SemanticKITTI. Enlarged numbered boxes show representative regions.

REFERENCES

- [1] Alexander Kirillov, Kaiming He, Ross Girshick, Carsten Rother, and Piotr Dollár, “Panoptic segmentation,” in *CVPR*, 2019.
- [2] Jonathan Long, Evan Shelhamer, and Trevor Darrell, “Fully convolutional networks for semantic segmentation,” in *CVPR*, 2015.
- [3] Shaoqing Ren, Kaiming He, Ross Girshick, and Jian Sun, “Faster R-CNN: Towards real-time object detection with region proposal networks,” in *NeurIPS*, 2015.
- [4] Rohit Mohan and Abhinav Valada, “EfficientPS: Efficient panoptic segmentation,” in *arXiv*, 2020.
- [5] Lorenzo Porzi, Samuel Rota Buló, Aleksander Colovic, and Peter Kotschieder, “Seamless scene segmentation,” in *CVPR*, 2019.
- [6] Bowen Cheng, Maxwell D Collins, Yukun Zhu, Ting Liu, Thomas S Huang, Hartwig Adam, and Liang-Chieh Chen, “Panoptic-DeepLab: A simple, strong, and fast baseline for bottom-up panoptic segmentation,” in *CVPR*, 2020.
- [7] Xinlong Wang, Shu Liu, Xiaoyong Shen, Chunhua Shen, and Jiaya Jia, “Associatively segmenting instances and semantics in point clouds,” in *CVPR*, 2019.
- [8] Quang-Hieu Pham, Thanh Nguyen, Binh-Son Hua, Gemma Roig, and Sai-Kit Yeung, “J3S3D: joint semantic-instance segmentation of 3D point clouds with multi-task pointwise networks and multi-value conditional random fields,” in *CVPR*, 2019.
- [9] Juana Valeria Hurtado, Rohit Mohan, and Abhinav Valada, “MOPT: Multi-object panoptic tracking,” in *CVPR Workshop*, 2020.
- [10] Andres Milioto, Jens Behley, Chris McCool, and Cyrill Stachniss, “LiDAR panoptic segmentation for autonomous driving,” in *IROS*, 2020.
- [11] Stefano Gasperini, Magdalini Paschali, Carsten Hopke, David Wittmann, and Nassir Navab, “Signal clustering with class-independent segmentation,” in *ICASSP*, 2020.
- [12] Daniel Maturana and Sebastian Scherer, “VoxNet: A 3D convolutional neural network for real-time object recognition,” in *IROS*, 2015.
- [13] Gernot Riegler, Ali Osman Ulusoy, and Andreas Geiger, “OctNet: Learning deep 3D representations at high resolutions,” in *CVPR*, 2017.
- [14] Andres Milioto, Ignacio Vizzo, Jens Behley, and Cyrill Stachniss, “RangeNet++: Fast and accurate LiDAR semantic segmentation,” in *IROS*, 2019.
- [15] Tiago Cortinhal, George Tzelepis, and Eren Erdal Aksoy, “SalsaNext: Fast semantic segmentation of LiDAR point clouds for autonomous driving,” in *arXiv*, 2020.
- [16] Charles R Qi, Hao Su, Kaichun Mo, and Leonidas J Guibas, “PointNet: Deep learning on point sets for 3D classification and segmentation,” in *CVPR*, 2017.
- [17] Charles Ruizhongtai Qi, Li Yi, Hao Su, and Leonidas J Guibas, “PointNet++: Deep hierarchical feature learning on point sets in a metric space,” in *NeurIPS*, 2017.
- [18] Qingyong Hu, Bo Yang, Linhai Xie, Stefano Rosa, Yulan Guo, Zhihua Wang, Niki Trigoni, and Andrew Markham, “RandLA-Net: Efficient semantic segmentation of large-scale point clouds,” in *CVPR*, 2020.
- [19] Alex H Lang, Sourabh Vora, Holger Caesar, Lubing Zhou, Jiong Yang, and Oscar Beijbom, “PointPillars: Fast encoders for object detection from point clouds,” in *CVPR*, 2019.
- [20] Hugues Thomas, Charles R Qi, Jean-Emmanuel Deschaud, Beatriz Marcotequi, François Goulette, and Leonidas J Guibas, “KPCConv: Flexible and deformable convolution for point clouds,” in *ICCV*, 2019.
- [21] Yifan Xu, Tianqi Fan, Mingye Xu, Long Zeng, and Yu Qiao, “Spider-CNN: Deep learning on point sets with parameterized convolutional filters,” in *ECCV*, 2018.
- [22] Deyvid Kochanov, Fatemeh Karimi Nejadasl, and Olaf Booij, “KPR-Net: Improving projection-based LiDAR semantic segmentation,” in *ECCV Workshop*, 2020.
- [23] Haotian Tang, Zhijian Liu, Shengyu Zhao, Yujun Lin, Ji Lin, Hanrui Wang, and Song Han, “Searching efficient 3D architectures with sparse point-voxel convolution,” in *ECCV*, 2020.
- [24] Kaiming He, Georgia Gkioxari, Piotr Dollár, and Ross Girshick, “Mask R-CNN,” in *ICCV*, 2017.
- [25] Bert De Brabandere, Davy Neven, and Luc Van Gool, “Semantic instance segmentation with a discriminative loss function,” in *arXiv*, 2017.
- [26] Davy Neven, Bert De Brabandere, Marc Proesmans, and Luc Van Gool, “Instance segmentation by jointly optimizing spatial embeddings and clustering bandwidth,” in *CVPR*, 2019.
- [27] Ji Hou, Angela Dai, and Matthias Nießner, “3D-SIS: 3D semantic instance segmentation of RGB-D scans,” in *CVPR*, 2019.
- [28] Li Yi, Wang Zhao, He Wang, Minhyuk Sung, and Leonidas J Guibas, “GSPN: Generative shape proposal network for 3D instance segmentation in point cloud,” in *CVPR*, 2019.
- [29] Feihu Zhang, Chenye Guan, Jin Fang, Song Bai, Ruigang Yang, Philip HS Torr, and Victor Prisacariu, “Instance segmentation of LiDAR point clouds,” in *ICRA*, 2020.
- [30] Yuwen Xiong, Renjie Liao, Hengshuang Zhao, Rui Hu, Min Bai, Ersin Yumer, and Raquel Urtasun, “UPSNet: A unified panoptic segmentation network,” in *CVPR*, 2019.
- [31] Konstantin Sofiiuk, Olga Barinova, and Anton Konushin, “AdaptIS: Adaptive instance selection network,” in *ICCV*, 2019.
- [32] Tien-Ju Yang, Maxwell D Collins, Yukun Zhu, Jyh-Jing Hwang, Ting Liu, Xiao Zhang, Vivienne Sze, George Papandreou, and Liang-Chieh Chen, “DeeperLab: Single-shot image parser,” in *arXiv*, 2019.
- [33] Naiyu Gao, Yanhu Shan, Yupei Wang, Xin Zhao, Yinan Yu, Ming Yang, and Kaiqi Huang, “SSAP: Single-shot instance segmentation with affinity pyramid,” in *ICCV*, 2019.
- [34] Jens Behley, Andres Milioto, and Cyrill Stachniss, “A benchmark for LiDAR-based panoptic segmentation based on KITTI,” in *arXiv*, 2020.
- [35] Maxim Berman, Amal Rannen Triki, and Matthew B Blaschko, “The Lovász-Softmax loss: A tractable surrogate for the optimization of the intersection-over-union measure in neural networks,” in *CVPR*, 2018.
- [36] Martin Ester, Hans-Peter Kriegel, Jörg Sander, Xiaowei Xu, et al., “A density-based algorithm for discovering clusters in large spatial databases with noise,” in *KDD*, 1996.
- [37] Jens Behley, Martin Garbade, Andres Milioto, Jan Quenzel, Sven Behnke, Cyrill Stachniss, and Jurgen Gall, “SemanticKITTI: A dataset for semantic scene understanding of LiDAR sequences,” in *ICCV*, 2019.
- [38] Andreas Geiger, Philip Lenz, and Raquel Urtasun, “Are we ready for autonomous driving? the KITTI vision benchmark suite,” in *CVPR*, 2012.